Lecture on

Biophysical aspects in sensing

Robert G. Endres*
Department of Life Sciences & Centre for Integrative Systems Biology and Bioinformatics, Imperial College, London SW7 2AZ, United Kingdom

While systems biology aims to understand the working and dynamics of molecules inside the cell, we mustn't forget that cells, although alive, follow physical laws. Hence, biophysical aspects are an important ingredient in modelling, and can also help building intuition regarding how processes work in biology. Here, I will show two examples of biophysical modelling in bacteria: (1) signal amplification and precise adaptation in chemotaxis, and (2) mechanosensitive ion channels and their gating by membrane tension.

Contents

I. BACTERIAL CHEMOTAXIS

Most types of cells are able to sense their environment and to migrate towards attractant chemicals (or away from repellent chemicals). Examples include single-cell organisms such as bacteria, amoeba, and yeast, as well as cells of our immune system, e.g. white blood cells, which chemotax towards sites of infections. Bacteria are particularly well-characterised with respect to their chemotactic properties [2], well known for sensing tiny changes in chemical concentration (down to 3 nM) and for adapting precisely to persistent changes.

To sense molecules in their environment, bacterial cells are equipped with different types of chemoreceptors, which can bind attractants (nutrients such as sugars and amino acids) and repellents (certain metal ions). In addition, they can also sense pH, oxygen, and temperature. Chemoreceptors exist in hundreds to thousands of copies and cluster predominatly at the cell poles. Fig. 1 shows examples of receptor clusters, imaged by fluorescence microscopy (panel A) [3] and electron microscopy (panels B and C) [4, 5]. These large clusters are known to act as "antennas", which amplify tiny changes in attactant concentration. This requires receptors to be coupled with their neighboring receptors. In addition to the receptors, a small signal transduction pathway relays the stimuli to the rotary motors, which drive the flagella for swimming. The pathway of *Escherichia coli*, an inhabitant of our intestines, is shown Fig. 2A.

In the *E. coli* chemotaxis pathway, active receptors, mainly Tar and Tsr, activate the receptor-bound kinase CheA to autophosphorylate, and subsequently pass the phosphate group on to the two response regulators, CheY and CheB. Phosphorylated CheY, i.e. CheY-P, diffuses through the cytoplasm and binds to the motors, inducing clockwise rotation. This leads to tumbling of the cell and random reorientation. If the receptors are inactive, the kinase does not autophosphoryate. Under such conditions, CheY is not phosphorylated, since phosphatase CheZ turns CheY-P to CheY, which does not bind to the motor. The motors are hence in their default mode of counter clock-wise rotation. This leads to bundling of the flagella, allowing the cell to run straight.

In order for cells to be able to sense new changes in chemical concentration, receptors and their signalling activity adapt. An adapted cell has always the same probability of tumbling, irrespective of the external chemical concentra-

* E-mail: r.endres@imperial.ac.uk

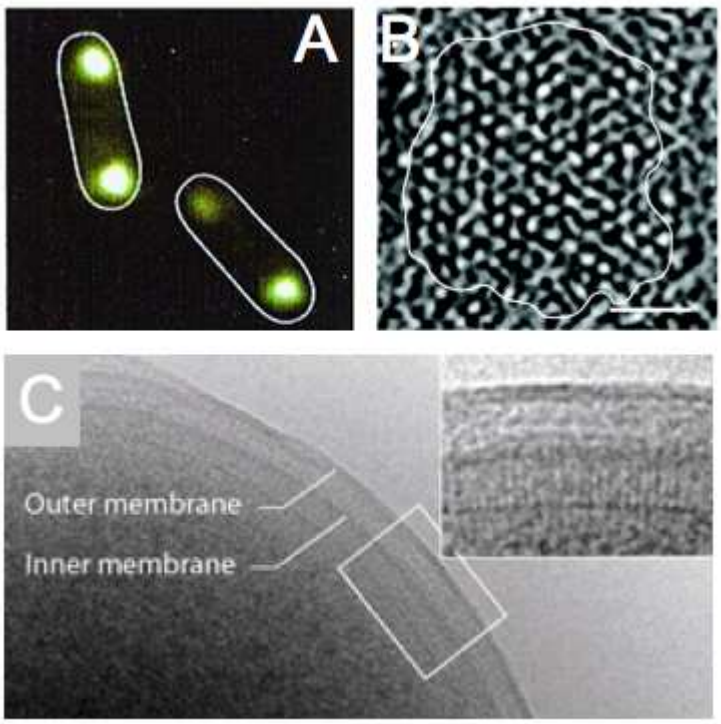

FIG. 1: Receptor clustering from fluorescence microscopy (A) and electron microscopy (B,C).

tion. For this purpose, enzyme CheR methylates the cytoplasmic part of the receptors, which increases the receptor signalling activity and the cell's probability of tumbling. There is also enzyme CheB, which, when phosphorylated, demethylates the receptors. This decreases the signalling activity and increases the cell's probability of running.

To study bacterial chemotaxis, researchers tracked swimming bacteria to record their runs and tumbles, or tethered cells with their motor or flagella to a glass slide to observe their direction of rotation. While these are powerful techniques, especially the latter, signalling can be measured in real time in living cells using fluorescence resonance energy transfer (FRET) [2]. For this purpose, one requires a donor fluorophore to be attached to one type of molecule in the pathway, and an acceptor fluorophore to another type of molecule as shown in Fig. 2A. These fluorophores are genetically attached to the proteins, and need to have specific optical properties. The donor fluorophore is excited by a laser at some wave length, and after excitation, emits the light again. However, when the acceptor comes close to the donor due to interactions in the signalling pathway, the acceptor can accept the excitation energy, and emit the light in a different, longer wave length. In bacterial chemotaxis, CheZ is fused to donor CFP and CheY is fused to acceptor YFP as shown in Fig. 2B. The ratio between the two fluorescence intensities is a measure of the signalling activity.

Using *in vivo* FRET, signalling and adaptation were quantified in detail [6]. In seminal work, step changes in attractant MeAsp, a nonmetabolizable analogue of aspartate and stimulator of the Tar receptor, are applied. Specifically, as shown in Fig. 3A cells are adapted to a background concentration of MeAsp and subsequently exposed to a step increase. After adaptation, the step is removed and cells adapt again to the original background concentration. Then, a new and larger step increase is applied and, after adaptation, is removed again and so forth. Recording the initial responses in activity (from FRET) results in dose-response curves shown in Fig. 3B. In this panel, filled symbols represent response to addition and open symbols represent response to removal of attractant. Immediately visible from these dose-response curves is that receptors have a high absolute sensitivity at zero concentration background (first addition curve), and become more and more insensitive at large background concentrations due to the increase in receptor methylation level.

The bacterial chemotaxis proteins are easily modified by genetics, allowing researchers to make cells, which, e.g., only express one receptor type, or receptors in specific fixed methylation-like states. The latter is possible since a glutamine (Q) behaves similarly to a methylated glutamate (E_m), since both are hydrophobic. Enzymes CheR and CheB also need to be removed from the chromosome so the remaining Es are not methylated. Using this technique, Fig. 4

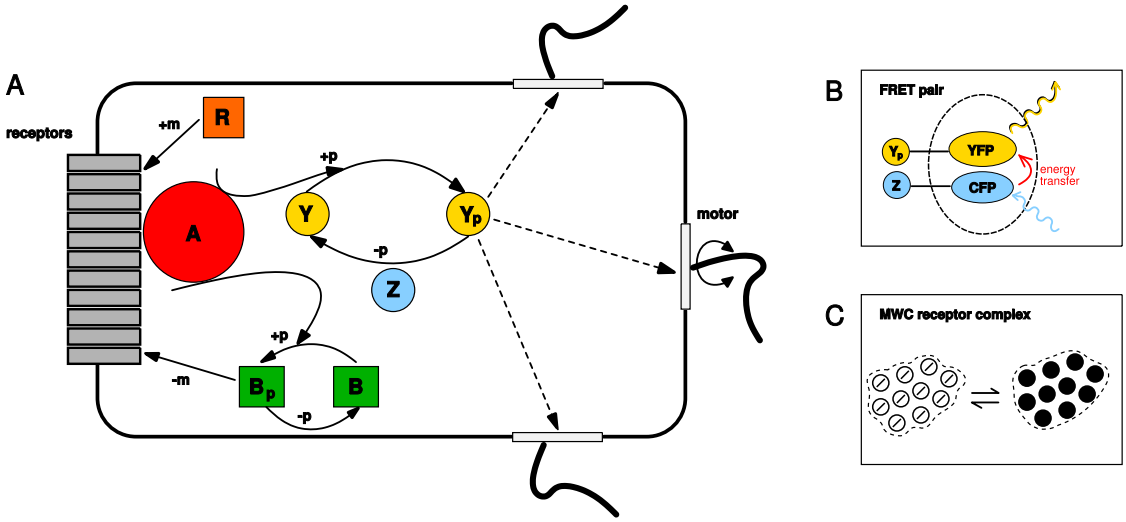

FIG. 2: *E. coli* chemotaxis pathway (A) and FRET assay (B). (C) Illustration of Monod-Wyman-Changeux (MWC) model for receptor cooperativity.

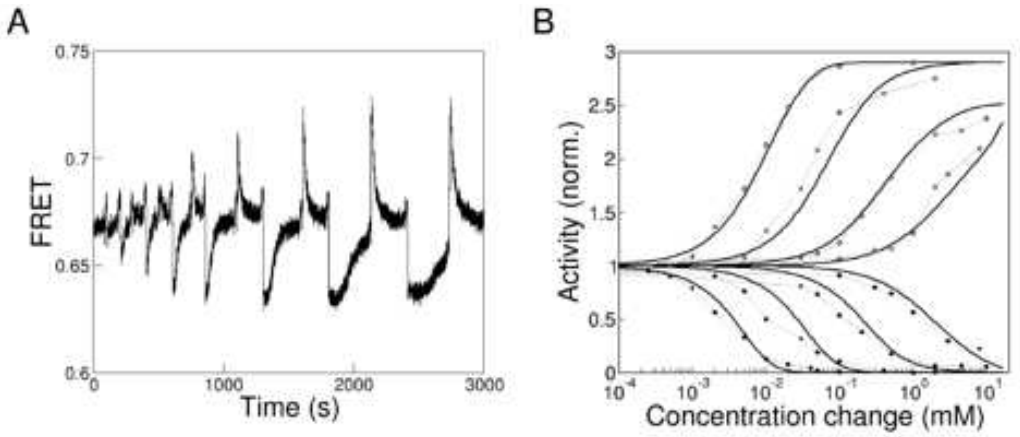

FIG. 3: Time-course data (A) and resulting dose-response curves (B) of adapting cells from FRET.

shows dose-response of cells expressing only Tar receptors in different "methylation states", indicated by the different amount of Es and Qs in the figure legend [7]. The figure also shows two dose-response curves of adapting Tar-only cells, initially adapted to cells zero and 0.1 mM MeAsp concentration background. These experiments with Tar-only cells show that there are large Hill coefficients for large methylation levels, pointing towards receptor-receptor cooperativity.

Recently, a model for signalling by cooperative receptors was proposed, which can describe the data very well (curves in Figs. 3B and 4) [7, 8]. The main assumptions, shown in Fig. 2C, are that (1) a number N of receptors forms a strongly coupled receptor complex, and that (2) receptors and hence complexes are two-state objects, which can either be in the *on* state, which signals, or in the *off* state which does not signal. Fig. 5 shows the free-energy profile of such a two-state receptor, describable by a single parameter $\Delta f = f_{\rm on} - f_{\rm off}$, which is the free-energy difference between the on and off states. The free-energy difference depends on ligand-receptor binding as well as receptor methylation. Since attractant inhibits the activity, ligand binding is taken to be stronger in the off-state than in the on-state of the receptor. Furthermore, receptor methylation favors the on-state, as methylation increases the activity.

Based on these assumptions, the free-energy difference is derived as follows, first for a single two-state receptor. As shown in Fig. 6, such a two-state receptor can be in four different states: (1) On without ligand bound, (2) on with ligand bound, (3) off without ligand bound, and (4) off with ligand bound. The energies of these four states are given

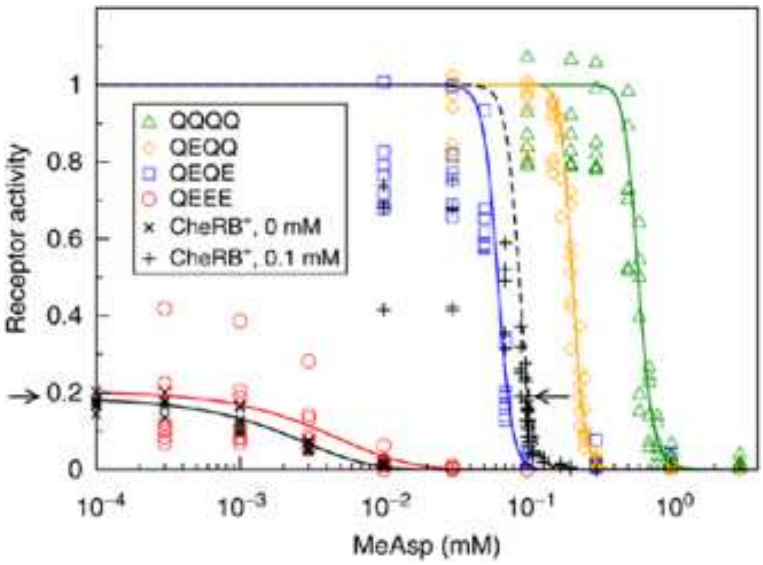

FIG. 4: Dose-response curves of non-adapting mutants from FRET (with fitted curves from MWC model).

by

$$E_{\rm on} \tag{1}$$

$$E^L_{\rm on} = E_{\rm on} - k_B T \ln\left(\frac{c}{K^{\rm on}_{\rm D}}\right) \tag{2}$$

$$E_{\rm off} \tag{3}$$

$$E^L_{\rm off} = E_{\rm off} - k_B T \ln\left(\frac{c}{K^{\rm off}_{\rm D}}\right), \tag{4}$$

where k_BT the thermal energy, c is the attractant concentration, and $K^{\rm on}_{\rm D}$ and $K^{\rm off}_{\rm D}$ are the ligand dissociation constants for the receptor in the on and off state, respectively. The ligand-bound energies emerge from the definition of the binding free energy, e.g. for the on state, $E^{bind}_{\rm on} = E^L_{\rm on} - E_{\rm on}$ and the experimentally known relation between the ligand dissociation constant and the binding free energy $K^{\rm on}_D = c \cdot e^{E_{\rm bind}/(k_BT)}$. The deeper origin of the last relation is in the competition between the energy release upon binding and the decrease in mixing entropy of the ligand in solution. Note also that in Eq. 2 the ligand-bound energy is very negative and hence favorable for $c \gg K^{\rm on}_D$, is equal to ligand-unbound energy $E_{\rm on}$ for $c = K^{\rm on}_D$, and is positive and hence unfavorable for $c \ll K^{\rm on}_D$.

To calculate the probability that the receptor is on/active, we invoke Boltzmann statistics, which tells us that the probability of finding the system in a state with energy E_i is $p_i = e^{-E_i/k_BT}/Z$, where Z is the partition function defined by $Z = \sum_i e^{-E_i/k_BT}$ [9, 10]. Using Boltzmann statistics in our example of the single receptor, the probability for the receptor to be on is given by

$$p_{\rm on} = \frac{e^{-E_{\rm on}} + e^{-E^L_{\rm on}}}{e^{-E_{\rm on}} + e^{-E^L_{\rm on}} + e^{-E_{\rm off}} + e^{-E^L_{\rm off}}} \tag{5}$$

$$= \frac{e^{-f_{\rm on}}}{e^{-f_{\rm on}} + e^{-f_{\rm off}}} \tag{6}$$

$$= \frac{1}{1 + e^{\Delta f}}, \tag{7}$$

where we expressed all energies in units of k_BT. In Eq. 6, the individual free energies are given by

$$f_{\rm on} = E_{\rm on} - \ln\left(1 + \frac{c}{K_{\rm D}^{\rm on}}\right) \tag{8}$$

$$f_{\rm off} = E_{\rm off} - \ln\left(1 + \frac{c}{K_{\rm D}^{\rm off}}\right), \tag{9}$$

and in Eq. 7, the free-energy difference is given by

$$\Delta f = \Delta E + \ln\left(\frac{1 + c/K_{\rm D}^{\rm off}}{1 + c/K_{\rm D}^{\rm on}}\right) \tag{10}$$

with $\Delta E = E_{\rm on} - E_{\rm off}$. Result Eq. 7 can be further simplified assuming that binding is very unfavorable in the on state, i.e. $K_D^{\rm on}$ is very large. In this case, we obtain

$$p_{\rm on} \approx \frac{1}{1 + e^{\Delta E}\left(1 + \frac{c}{K_D^{\rm off}}\right)}. \tag{11}$$

Now, if there are N receptors in a complex, which are so strongly coupled so they are always all on or off together, then Eq. 5 reads

$$p_{\rm on} = \frac{(e^{-E_{\rm on}} + e^{-E_{\rm on}^L})^N}{(e^{-E_{\rm on}} + e^{-E_{\rm on}^L})^N + (e^{-E_{\rm off}} + e^{-E_{\rm off}^L})^N} \tag{12}$$

$$= \frac{e^{-F_{\rm on}}}{e^{-F_{\rm on}} + e^{-F_{\rm off}}} \tag{13}$$

$$= \frac{1}{1 + e^{\Delta F}} \tag{14}$$

$$\approx \frac{1}{1 + e^{N\Delta E}\left(1 + \frac{c}{K_D^{\rm off}}\right)^N} \tag{15}$$

where

$$F_{\rm on} = N\left[E_{\rm on} - \ln\left(1 + \frac{c}{K_{\rm D}^{\rm on}}\right)\right] \tag{16}$$

$$F_{\rm off} = N\left[E_{\rm off} - \ln\left(1 + \frac{c}{K_{\rm D}^{\rm off}}\right)\right] \tag{17}$$

and

$$\Delta F = N\left[\Delta E + \ln\left(\frac{1 + c/K_{\rm D}^{\rm off}}{1 + c/K_{\rm D}^{\rm on}}\right)\right]. \tag{18}$$

As evident from the receptor with specific methylation levels in Fig. 4, there are two regimes of signalling in the data [8]. Demethylated receptors are highly sensitive and have a low activiy at low attractant concentration. In contrast, methylated receptors are very insensitive, are very active at low attractant concentration, and exhibit large cooparativity. In the following, we will show that these two regimes are indeed predicted by the model.

Regime I: $E_{\rm on} \gg E_{\rm off}$ ($\Delta E \gg 0$)
In this regime, we can neglect the number one in the denominator of Eq. 15, and obtain

$$p_{\rm on} = \frac{e^{-N\Delta E}}{\left(1 + c/K_D^{\rm off}\right)^N}, \tag{19}$$

leading to

$$p_{\rm on}^{\rm max}(c = 0) = e^{-N\Delta E}. \tag{20}$$

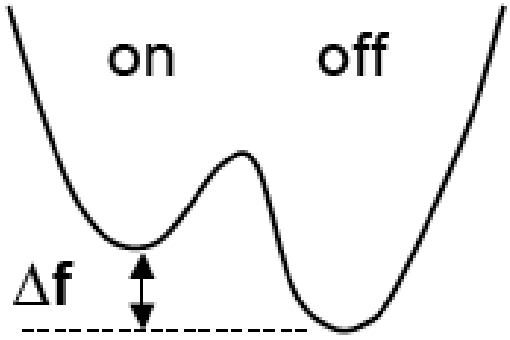

FIG. 5: Free-energy profile of a two-state receptor.

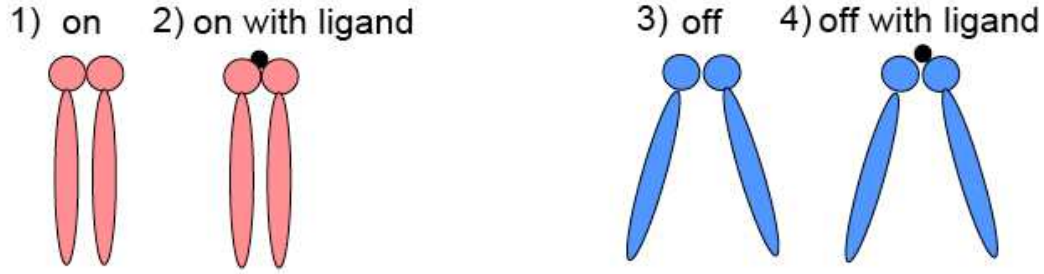

FIG. 6: A two-state receptor has four microstates.

To derive the inhibition constant K_i, i.e. the ligand concentration for which receptor activity is half of the maximal activity, we set $p_{\rm on} = e^{-N\Delta E}/2$ in Eq. 19 and solve for c. This gives $K_i = K_D^{\rm off} \ln 2/N$. Hence, a receptor complex is N times more sensitive than a single receptor.

Regime II: $E_{\rm on} \ll E_{\rm off}$ ($\Delta E \ll 0$)
Using $p_{\rm on} \approx 1/2$ in Eq. 15 results in

$$e^{N\Delta E}\left(1 + c/K_D^{\rm off}\right)^N = 1 \tag{21}$$

and finally $K_i = K_D^{\rm off} e^{|\Delta E|}$, which increases with methylation as $|\Delta E|$ increases with methylation. Furthermore, for $c \gg K_D^{\rm off}$, we obtain a Hill-type equation

$$p_{\rm on} \approx \frac{1}{1 + \left(e^{\Delta E}\frac{c}{K_D^{\rm off}}\right)^N}, \tag{22}$$

where the complex size N plays the role of the Hill coefficient.

Precise adaptation. As shown in Fig. 3A, adaptation to persistent stimulation, such as a step increase of attractant, is very precise. The two-state model for signalling also proposes an elegant way of achieving this remarkable feature [11]. Specifically, there are three different ways of looking at adaptation: (1) The free-energy landscape picture, shown in Fig. 5, in which ligand favors (lowers) the off state minimum and subsequent methylation lowers the on state minimum to re-gain correct Δf. However, this does not explain how receptor methylation stops at the right moment to achieve this. (2) The dynamics picture. Naively, we would be tempted to write down dynamics such as

$$\frac{dm}{dt} = k_R \cdot R \cdot c \cdot (m_{\rm max} - m) \;-\; k_B \cdot B \cdot p_{\rm on}(c, m) \cdot m, \tag{23}$$

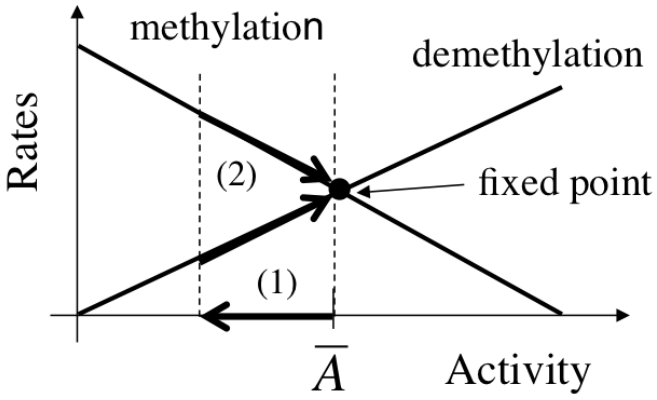

FIG. 7: Robust precise adaptation explained by a stable fixed point: An increase in c leads to a temporary decrease in $A = p_{\rm on}$ (1), but methylation rate is then larger than demethylation rate, bringing system back to adapted value (2). This value is a stable fixed point of the underlying dynamics.

where rate of methylation depends, in addition on stimulus c, on number of available methylation sites (substrate) and the rate of demethylation depends on number of methyl groups (substrate again). However, this model would produce an adapted steady-state methylation level depending on c. The resulting activity could be anything, which is not precise adaptation. The correct activity value could be achieved by fine tuning but this would not work robustly over a wide range of c values. Instead, if the dynamics of receptor methylation only depend on the activity of the receptors, and not on the number of available sites for methylation or demethylation, or the external attractant concentration, adaptation always returns the activity back to the same adapted activity. For instance, the dynamics may be given by

$$\frac{dm}{dt} = k_R(1 - p_{\rm on}) \; - \; k_B p_{\rm on}, \tag{24}$$

where k_R is the rate of methylation, including the concentration of CheR, and k_B is the rate of demethylation, including the concentration of active CheB. Evidently, Eq. 24 does not depend directly on the receptor methylation level or attractant concentration, only indirectly on these through $p_{\rm on}$. At steady-state, i.e. after adaptation, $dm/dt = 0$ and the right-hand side of Eq. 24 can be solved for the steady-state activity

$$p^*_{\rm on} = \frac{k_R}{k_R + k_B}, \tag{25}$$

which only depends on intrinsic rate parameters and hence is independent of external conditions of the cell. Hence, the adapted activity is a stable fixed point of the underlying dynamics, at which methylation and demthylation rates balance each other exactly (see Fig. 7).

Yet another way, (3), of looking at precise adaptation is via *integral feedback control* [12]. This is a well-known engineering control mechanism to track the correct temperature in an oven or a room. Here, instead of adding temperature when it happens to be too low, which leads to oscillations and hence instability, temperature is added when the time integral of the temperature is too low (when it is too low on average), i.e. $\Delta Q \sim \int \Delta T(t) dt$. Analogously, in bacterial chemotaxis the number of added (or removed) methyl groups is proportional to the integrated error of the activity. To see this, we linearise Eq. 24 by introducing fluctuations from steady state $m(t) = \bar{m} + \delta m(t)$ and $p_{\rm on}(t) = \bar{p}_{\rm on} + \delta p_{\rm on}(t)$. This leads to

$$\frac{d(\delta m)}{dt} = -\lambda \delta p_{\rm on} \tag{26}$$

with relaxation rate $\lambda = k_R + k_B$. Integration finally demonstrates integral feedback control:

$$\Delta m = \int d(\delta m) = -\lambda \int \delta p_{\rm on}(t) dt. \tag{27}$$

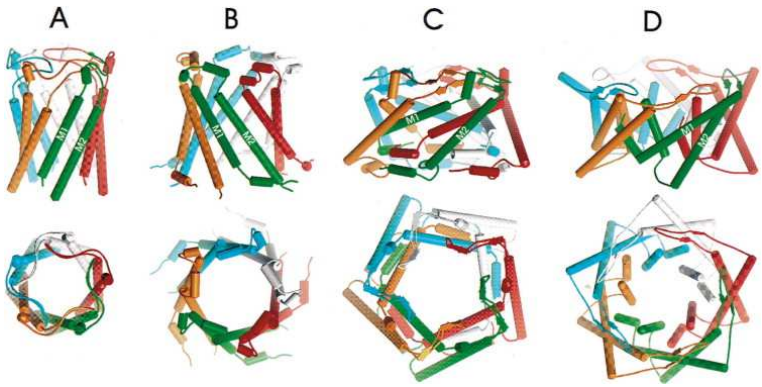

FIG. 8: Crystal structures of open and closed conformations of MscL channel.

II. MECHANOSENSITIVE ION CHANNELS

The membrane of a cell with its embedded proteins plays an active role in regulating homeostasis of the cell. In addition to receptors, bacteria have mechanosensitive ion channels which serve as a safety valve to protect the cell against membrane rupture due to osmotic imbalance. In particular, when the bacterium is under osmotic shock, e.g. by putting a cell into pure water, the resulting influx of water across the cell membrane results in a rapid increase in membrane tension. These channels reply by opening and allowing ions and small molecules to leave the cell, thus saving the cell from bursting. The Mechanosensitive Channel of Large Conductance (MscL) protein is a model system which permits the study of how gating of the channel is tied to membrane deformation and external tension [10, 13, 14].

Figure 8 shows the open and closed states (as well as intermediates) obtained from X-ray crystallography, and Fig. 9 demonstrates that the probability for the channel to be in the open conformation decreases with the engineered length of the hydrophobic tail of the lipids, which make up the membrane. This shows that the channel cannot be considered as an isolated object but is gated by the membrane properties.

To understand how membrane tension can gate the opening and closing of an ion channel, we need to know that ion channels, like other membrane embedded proteins, have a hydrophobic region of amino acids, which anchors the protein in the membrane (Fig. 10). If the hydrophobic region is smaller than the width of the membrane as shown in Fig. 9, the width of the lipid bilayer will shrink to match the protein region. In constrast, if the hydrophobic region is larger than the width of the membrane, the width of the lipid bilayer will expand correspondingly. Hence, the protein, simplified as a solid object, deforms the membrane around it. This costs some bending and stretching energy, but is offset by the hydrophobic attraction between the hydrophobic lipid tails and hydrophobic protein region.

Before explaining the effects of gating by membrane tension, we will calculate the deformation of the membrane around the channel and the energy of the channel-membrane system. While the membrane is a two-dimensional sheet, we make the assumption that the channel radius is rather large, so that we can consider the approximate one-dimensional case shown in Fig. 11A. Once this is achieved, we will approximate the two-dimensional solution by wrapping the membrane around the channel as indicated in Figs. 11B and C.

In the one-dimensional case, the width of the hydrophobic region of the channel is W and the width of one lipid layer is $w(x)$, where x is the distance from the channel circumference. Now, introducing variable $u(x) = w(x) - w_0$, which measures the lipid deformation away from its equilibrium value w_0, we can write the energy of the membrane as

$$E[u(x)] = \underbrace{\frac{K_b}{2}\int_R^\infty \left(\frac{d^2u}{dx^2}\right)^2 dx}_{\text{bending energy}} + \underbrace{\frac{K_t}{2w_0^2}\int_R^\infty u(x)^2 dx}_{\text{stretching energy}}, \tag{28}$$

where notation $E[u(x)]$ indicates that the energy is a functional of $u(x)$. Furthermore, the first term on the right-hand side is the bending energy and the second denotes the stretching energy of the lipid bilayer to match the protein region. In order to compute the energy associated with the membrane deformation, we must find the profile $u(x)$ that minimizes this energy subject to the boundary conditions. When solving a differential equation like that one derived

from Eq. 28, we have to say something about how the value of $u(x)$ at the boundaries $x = R$, i.e. the channel radius, and for $x \to \infty$. At $r = R$, we assume strong hydrophobic "gluing"

$$u(R) = \frac{W}{2} - w_0 = U, \tag{29}$$

and that the derivative is zero

$$u'(R) = 0. \tag{30}$$

Furthermore, we make the realistic assumption that for $x \to \infty$ the membrane becomes the unperturbed membrane

$$u(\infty) = 0 \tag{31}$$
$$u'(\infty) = 0. \tag{32}$$

Minimization of the energy functional is analogous to minimizing an ordinary function by setting the derivative equal to zero. Here, we set the functional derivative to zero and obtain a differential equation. To compute the function drivative, we let the function $u(x)$ undergo a small excursion $\eta(x)$ by substituting $u(x) \to u(x) + \epsilon\eta(x)$ with the boundary conditions on u that η vanishes at the boundaries. The functional derivative is defined as

$$\frac{\partial E}{\partial u(x)} = \lim_{\epsilon \to 0} \frac{E[u(x) + \epsilon\eta(x), u''(x) + \epsilon\eta''(x)] - E[u(x), u''(x)]}{\epsilon}, \tag{33}$$

with $u'' = d^2u/dx^2$ and similarly for η''. Denoting the integrand in Eq. 28 as f, that is $E[u(x)] = \int_R^\infty f(u'', u)dx$, we Taylor expand

$$f[u + \epsilon\eta, u'' + \epsilon\eta''] \approx f[u, u''] + \epsilon\frac{\partial f}{\partial u}\eta + \epsilon\frac{\partial f}{\partial u''}\eta'' \tag{34}$$

with the first term being cancelled in Eq. 33 (by taking the difference in Eq. 33). We thus obtain the functional derivative

$$\frac{\partial E}{\partial u(x)} = \int_R^\infty \left(\frac{\partial f}{\partial u''}\eta'' + \frac{\partial f}{\partial u}\eta\right) dx = 0 \tag{35}$$
$$\to K_b \int_R^\infty u''\eta''dx + \frac{K_t}{w_0^2}\int_R^\infty u\,\eta\,dx = 0. \tag{36}$$

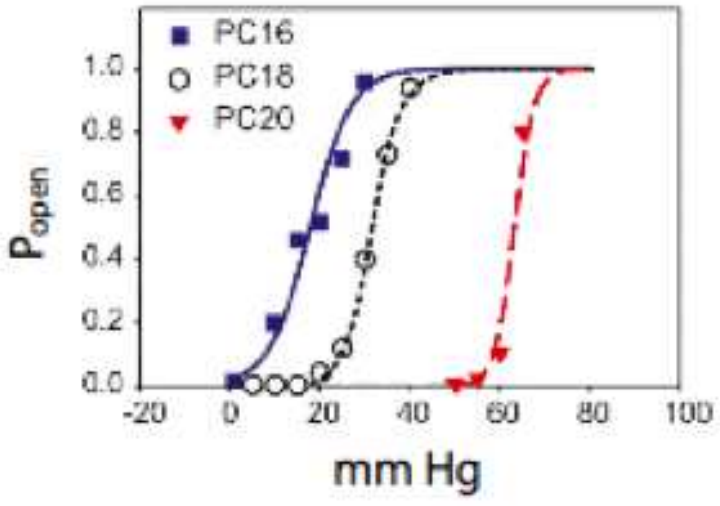

FIG. 9: Open probability of MscL as a function of pressure for different membrane thicknesses.

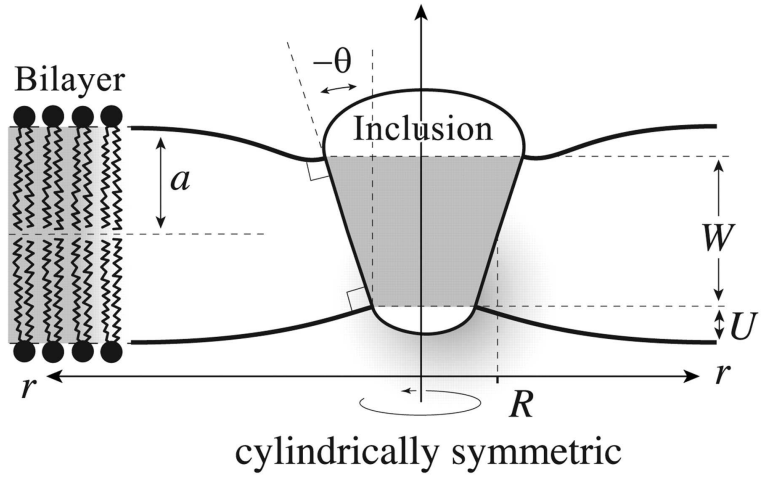

FIG. 10: Membrane thickness tries to match hydrophobic transmembrane protein region [13].

FIG. 11: Extending model from 1D to 2D (valid for large channel) [10].

We proceed by integrating by parts the first term, resulting in

$$K_b u''\eta'|_R^\infty - K_b \int_R^\infty u'''\eta' dx \; + \; \frac{K_t}{w_0^2}\int_R^\infty u\,\eta\, dx = 0. \tag{37}$$

The first term is zero as η' vanishes at the boundaries. We can integrate by parts once more and obtain

$$-K_b u'''\eta|_R^\infty + K_b \int_R^\infty u''''\eta dx \; + \; \frac{K_t}{w_0^2}\int_R^\infty u\,\eta\, dx = 0, \tag{38}$$

where the first term vanishes again. Since this integral is zero for any η, we obtain the forth-order differential equation

$$K_b \frac{d^4u}{dx^4} + \frac{K_t}{w_0^2}u = 0. \tag{39}$$

with its solution delivering the membrane profile which minimizes the energy of the membrane around the channel. To solve Eq. 39, we make an *Ansatz* of the form $u = e^{\Lambda x}$, leading to

$$\Lambda^4 + \frac{K_t}{K_b w_0^2} = 0 \tag{40}$$

and

$$\Lambda = \sqrt[4]{\frac{K_t}{K_b w_0^2}} \times \sqrt[4]{-1}. \tag{41}$$

The 4th root of -1 can easily be calculated by using the Euler formula $e^{i\theta} = \cos\theta + i\sin\theta$, i.e. $e^{i\pi} = -1$ in our case, and realising that there are an infinite number of solutions $e^{i(2n+1)\pi} = -1$ for $n = 0, 1, 2, ...$ However, the four

distinct solutions are $n = 0, 1, 2, 3$, and 4, leading to angles $\pi/4$, $3\pi/4$, $5\pi/4$, and $7\pi/4$, and

$$\Lambda_1 = \sqrt[4]{\frac{K_t}{K_b w_0^2}} e^{i\pi/4} = \sqrt[4]{\frac{K_t}{K_b w_0^2}} \left(\frac{\sqrt{2}}{2} + i\frac{\sqrt{2}}{2} \right) \tag{42}$$

$$\Lambda_2 = \sqrt[4]{\frac{K_t}{K_b w_0^2}} e^{i3\pi/4} = \sqrt[4]{\frac{K_t}{K_b w_0^2}} \left(-\frac{\sqrt{2}}{2} + i\frac{\sqrt{2}}{2} \right) \tag{43}$$

$$\Lambda_3 = \sqrt[4]{\frac{K_t}{K_b w_0^2}} e^{i5\pi/4} = \sqrt[4]{\frac{K_t}{K_b w_0^2}} \left(-\frac{\sqrt{2}}{2} - i\frac{\sqrt{2}}{2} \right) \tag{44}$$

$$\Lambda_4 = \sqrt[4]{\frac{K_t}{K_b w_0^2}} e^{i7\pi/4} = \sqrt[4]{\frac{K_t}{K_b w_0^2}} \left(\frac{\sqrt{2}}{2} - i\frac{\sqrt{2}}{2} \right). \tag{45}$$

Choosing the two solutions with negative real part for decay far away from the membrane-embedded channel, we obtain

$$u(x) = C_2 e^{\Lambda_2 x} + C_3 e^{\Lambda_3 x} \tag{46}$$

with constants C_2 and C_3 to be determined using the boundary conditions. Applying the boundary conditions leads two algebraic equations

$$C_2 e^{\Lambda_2 R} + C_3 e^{\Lambda_3 R} = U \tag{47}$$

$$\Lambda_2 C_2 e^{\Lambda_2 R} + \Lambda_3 C_3 e^{\Lambda_3 R} = 0, \tag{48}$$

which can be solved and, plugged into Eq. 46, produce the final solution

$$u(x) = U e^{-(\sqrt{2}/2)\lambda(x-R)} \left[\cos\frac{\sqrt{2}}{2}\lambda(x-R) + \sin\frac{\sqrt{2}}{2}\lambda(x-R) \right] \tag{49}$$

with

$$\lambda = \sqrt[4]{\frac{K_t}{K_b w_0^2}}. \tag{50}$$

To calculate the energy Eq. 28, we need the second derivate

$$u''(x) = U\lambda^2 e^{-(\sqrt{2}/2)\lambda(x-R)} \left[\sin\frac{\sqrt{2}}{2}\lambda(x-R) - \cos\frac{\sqrt{2}}{2}\lambda(x-R) \right] \tag{51}$$

and solve the resulting integral

$$E = \frac{K_b}{2} \int_R^\infty dx\, U^2 \lambda^4 e^{-\sqrt{2}\lambda(x-R)} \left[1 - 2\sin\frac{\sqrt{2}}{2}\lambda(x-R) \times \cos\frac{\sqrt{2}}{2}\lambda(x-R) \right] \tag{52}$$

$$+ \frac{K_t}{2w_0^2} \int_R^\infty dx\, U^2 e^{-\sqrt{2}\lambda(x-R)} \left[1 + 2\sin\frac{\sqrt{2}}{2}\lambda(x-R) \times \cos\frac{\sqrt{2}}{2}\lambda(x-R) \right] \tag{53}$$

$$= \frac{K_t U^2}{\omega_0^2} \int_R^\infty dx\, e^{-\sqrt{2}\lambda(x-R)} = \frac{K_t U^2}{\sqrt{2}\lambda w_0^2}. \tag{54}$$

The total energy of the channel-membrane system with an applied membrane tension τ, e.g. due to osmotic pressure,

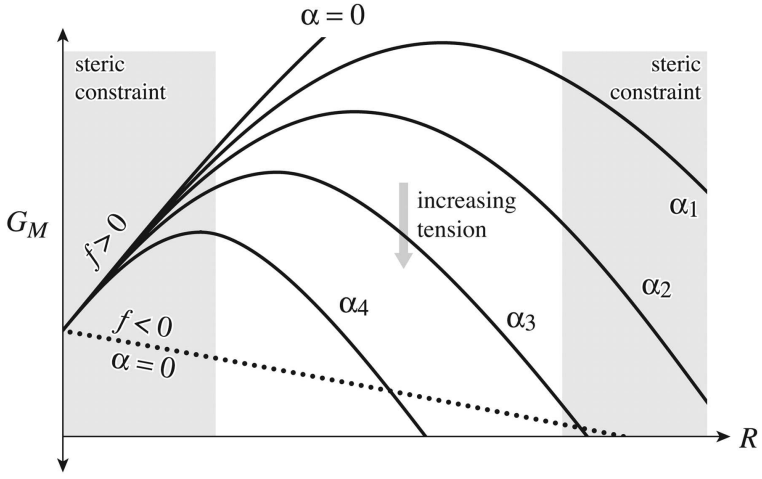

FIG. 12: Model results for gating by membrane tension [13].

is

$$E_{\mathrm{MscL}} = E + E_{\mathrm{tension}} \tag{55}$$

$$= E_0 + \underbrace{\frac{K_t U^2}{\sqrt{2} w_0^2 \lambda}}_{\text{energy/length}} \underbrace{2\pi R}_{\text{circumference}} - \underbrace{\tau \pi R^2}_{\text{loading device}} \tag{56}$$

$$= E_0 + \frac{1}{2} K U^2 2\pi R - \tau \pi R^2 \tag{57}$$

with

$$K = \sqrt{2} \sqrt[4]{\frac{K_t^3 K_b}{w_0^6}}. \tag{58}$$

In this equation, an overall additive constant E_0 is left undetermined. Notice the second term is positive and proportial to channel radius R, hence describing a line tension. In contrast, the third term is negative and proportional to R^2, as required for a proper surface tension. As a result, the total energy is parabolic with respect to R as shown in Fig. 11. For small tension, the closed state is favorable (lower) in energy, while for large tension, the open state is more favorable.

[1] Endres RG, Physical principles in sensing and signaling (Oxford, 2013).
[2] Sourjik V (2004) Receptor clustering and signal processing in *E. coli* chemotaxis. Trends Microbiol **12**: 569.
[3] Gestwicki JE *et al.* (2000) Evolutionary conservation of methyl-accepting chemotaxis protein location in Bacteria and Archaea. J Bacteriol **182**: 6499.
[4] Zhang P *et al.* (2007) Direct visualization of *Escherichia coli* chemotaxis receptor arrays using cryo-electron microscopy. Proc Natl Acad Sci USA **104**: 3777.
[5] Khursigara CM, Wu X, Subramaniam S (2008) Chemoreceptors in *Caulobacter crescentus*: trimers of receptor dimers in a partially ordered hexagonally packed array. J Bacteriol **190**: 6805.
[6] Sourjik V, Berg HC (2002) Receptor sensitivity in bacterial chemotaxis. Proc Natl Acad Sci USA **99**: 123.
[7] Endres RG, Oleksiuk O, Hansen CH, Meir Y, Sourjik V, Wingreen NS (2008) Variable sizes of *Escherichia coli* chemoreceptor signaling teams. Mol Syst Biol **4**: 211.
[8] Keymer JE, Endres RG, Skoge M, Meir Y, Wingreen NS (2006) Chemosensing in *Escherichia coli*: two regimes of two-state receptors. Proc Natl Acad Sci USA **103**: 1786.
[9] Berg HC, Random walk in biology (Princeton University Press, 1993).
[10] Phillips R, Kondev J, Theriot J (2004) Physical Biology of the Cell (Garland Science).
[11] Barkai N, Leibler S (1997) Robustness in simple biochemical networks. Nature **387**: 913.

[12] Yi TM, Huang Y, Simon MI, Doyle J (2000) Robust perfect adaptation in bacterial chemotaxis through integral feedback control. Proc Natl Acad Sci USA **97**: 4649.
[13] Wiggins P, Phillips R (2004) Analytic models for mechanotransduction: gating a mechanosensitive channel. Proc Natl Acad Sci USA **101**: 4071.
[14] Ursell T, Kondev J, Reeves D, Wiggins PA, Phillips R (2008) *Role of Lipid Bilayer Mechanics in Mechanosensation* in *Mechanosensitive Ion Channels*, Eds.: Kamkin A, Kiseleva I (Springer)